Journal of Magnetic Resonance 198 (2009) 8–14

Contents lists available at ScienceDirect

Journal of Magnetic Resonance

journal homepage: www.elsevier.com/locate/jmr

Segmented surface coil resonator for in vivo EPR applications at 1.1 GHz

Sergey Petryakov, Alexandre Samouilov, Michael Chzhan-Roytenberg, Eric Kesselring, Ziqi Sun, Jay L. Zweier *

Center for Biomedical EPR Spectroscopy and Imaging, Davis Heart & Lung Research Institute and the Division of Cardiovascular Medicine, Department of Internal Medicine, The Ohio State University College of Medicine, Columbus, OH 43210, USA

ARTICLE INFO

Article history:
Received 24 September 2008
Revised 3 December 2008
Available online 24 December 2008

Keywords:
EPR
L-band
Surface coil
Resonator
Co-imaging

ABSTRACT

A four-loop segmented surface coil resonator (SSCR) with electronic frequency and coupling adjustments was constructed with 18 mm aperture and loading capability suitable for in vivo Electron Paramagnetic Resonance (EPR) spectroscopy and imaging applications at L-band. Increased sample volume and loading capability were achieved by employing a multi-loop three-dimensional surface coil structure. Symmetrical design of the resonator with coupling to each loop resulted in high homogeneity of RF magnetic field. Parallel loops were coupled to the feeder cable via balancing circuitry containing varactor diodes for electronic coupling and tuning over a wide range of loading conditions. Manually adjusted high Q trimmer capacitors were used for initial tuning with subsequent tuning electronically controlled using varactor diodes. This design provides transparency and homogeneity of magnetic field modulation in the sample volume, while matching components are shielded to minimize interference with modulation and ambient RF fields. It can accommodate lossy samples up to 90% of its aperture with high homogeneity of RF and modulation magnetic fields and can function as a surface loop or a slice volume resonator. Along with an outer coaxial NMR surface coil, the SSCR enabled EPR/NMR co-imaging of paramagnetic probes in living rats to a depth of 20 mm.

Published by Elsevier Inc.

1. Introduction

Increasing interest in application of EPR spectroscopy and imaging techniques for the study of the kinetics and spatial distribution of free radicals and oxygen in in vivo biological tissues and animals has generated a great demand for development of EPR sample resonators capable of accommodating large lossy biological samples [1–8]. The need to achieve the highest sensitivity in the presence of motional noise from breathing and animal movements necessitated the development of resonators with active compensation of frequency and coupling by employing circuitry for Automatic Tuning Control (ATC) and Automatic Coupling Control (ACC). Surface coil resonators (SCR) with ATC and ACC utilizing electric coupling circuit designs have been extensively researched and developed [9–11]. These can be used with the sample placed enface as surface resonators or with sample placed within the loop as a slice selective volume resonator. These employ electric coupling circuits of symmetrical design allowing the widest range of frequency and coupling adjustment by means of voltage adjustment applied to corresponding varactor diodes. In practical applications of such resonators for in vivo EPR spectroscopy and imaging, high-level compensation of motional noise was achieved [9–11]. However, this design has certain limitations. In order to perform EPR measurements on larger animals and humans, further development and improvements in surface coil or volume coil resonator design are required to address several critical needs. These include:

1. The need to accommodate larger samples. Surface coil resonators currently available for use in L-band (typically around 1.2 GHz) are limited to useful apertures of less than 10 mm [1,7,12–14]. The diameter for conventional single loop surface coils is limited by frequency to about one quarter wave length in the conductor [7].
2. The need for increased depth of field penetration within the sample. Current L-band SCRs are limited to about 2–3 mm depth of RF field penetration [4,8,9,11,13,15]; for larger in vivo applications there is a need for measurements on deeper structures.
3. The need for improvement of the homogeneity of B_1 field distribution. A single loop resonator has an inherent asymmetric field distribution, since the electric field is concentrated near the ends of the loop [13]. A multi-loop resonator design has the potential to overcome these limitations.

Constructing the surface loop resonator with increased aperture raises several problems which must be overcome including:

* Corresponding author. Fax: +1 614 247 7845.
E-mail address: jay.zweier@osumc.edu (J.L. Zweier).

1090-7807/$ - see front matter Published by Elsevier Inc.
doi:10.1016/j.jmr.2008.12.014

1. The need for enhanced mechanical stability to suppress microphonic noise. With the increased dimensions of a multi-loop resonator, enhanced mechanical and vibrational stability is required.
2. The need to maximize modulation field homogeneity. Though the surface loop design is inherently transparent to field modulation, further improvements are required to maximize modulation field homogeneity and minimize direct coupling of the loop to the modulation field.
3. The need for enhanced coupling efficiency and stability at higher applied power. The increased volume of lossy samples requires a proportional increase in applied power, necessitating enhancements in coupling efficiency and stability of the automatic tuning and coupling circuits.

The four-loop segmented surface coil resonator (SSCR) and coupling circuit described below was developed to address these concerns and circumvent these limitations.

2. Resonator design

To overcome the inherent size limitations of the single loop coaxial cable resonator, a novel multi loop coaxial cable surface resonator was developed and tested. The general concept of this resonator is schematically shown in Fig. 1 (a four-segment resonator is shown). The inductive loop of this resonator is formed by four identical loop segments (a) connected in series with respect to RF current in the loop. This allows increasing the diameter of the resulting loop. In principal, the number of loop segments may be increased to attain larger diameter at a given frequency. This number must be even for symmetry of the resonator circuit with respect to the signal ground. An additional benefit of this design is its greater mechanical stability than a conventional single loop resonator whose rigidity is based only on a single pair of semi-rigid coaxial cables [10]. Implementation of the three-dimensional SSCR design results in enhanced rigidity and reduced susceptibility to acoustical/vibrational interference from living animals or external sources.

The identical loops formed by conductors "a" and "b" are connected in parallel with respect to the coupling circuit. Fig. 2 shows the schematics of the resonator with coupling circuit. Four segments of the loop are comprised of four identical elements shaped from 50-Ω semi-rigid coaxial cable. (Micro-Coax - UT-141C PTFE non-magnetic cable with copper jacket and center conductor; outer diameter 3.6 mm, center conductor diameter 0.9 mm.) For each element the outer coaxial shield was removed in the center region at 23 mm length (element "a" at Fig. 1A). The original Teflon dielectric around the unshielded sections was left intact in order to prevent a contact of the wire with the sample and avoid potential contamination. The equal lengths of the cables on both sides of the exposed center conductor are 110 mm each. The lengths are such that each element forms a 3/4 wavelength resonance circuit with serially connected capacitors at the resonance frequency of the resonator, approximately 1.1 GHz. Final coaxial sections length adjustments were performed to achieve the exact desired frequency. Combined together, the four elements resonate at this frequency and form a loop of ~20 mm in diameter with usable diameter of 18 mm. The resulting structure was integrated within a glass epoxy composite body (element "c" in Fig. 1). The thin silver conducting coating was applied to the body to provide RF shielding while being transparent to the modulation frequency magnetic field. The hardened epoxy resin has high dielectric loss coefficient, and silver metallization was used to prevent RF electric field penetration into its volume and degradation of the resonator *Q*-factor due to dielectric losses in the epoxy volume.

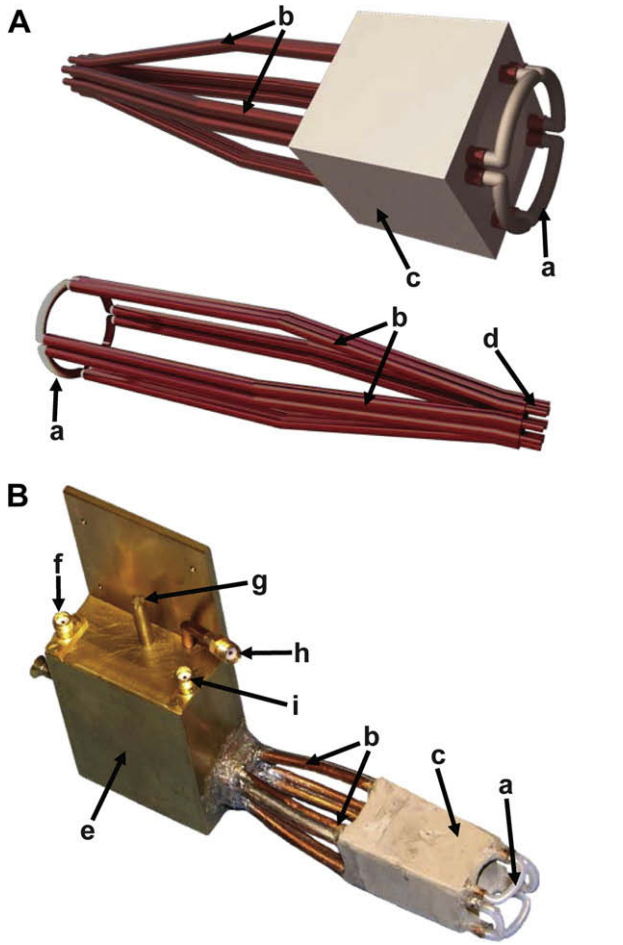

Fig. 1. General design concept and photograph of the segmented surface coil resonator (SSCR). Four-loop design is shown. In Fig. 1A, the top drawing shows the resonator loops and feeding lines with glass-epoxy composite frame and the lower drawing a view of the resonator from opposite side without the composite frame. (a) Segment of the resonator loop formed by removing the shield from the middle section of 50 Ω semi-ridged coaxial cable. (b) Feeding lines of the loop segment (a). (c) Structural frame. (d) Contact of the resonator loop. (B) The photo of the four-loop SSCR. The resonator is shown with coupling circuit enclosure (e) attached. (c) Structural frame; (f) electronic coupling control input; (g) manual coupling control screw; (h) RF feeding cable; (i) electronic tuning control input; (e) enclosure for coupling circuit. Of note, while the proposed structure of the loop was circular, with the limited deformability of the semi rigid coaxial cable used, the arrangement of the four loops as seen in (B) appears square.

By carefully designing the resonator structure in a way that no short circuits with respect to the modulation field exist, we have achieved "transparency" and homogeneity of the modulation field. The plane of the surface loop is perpendicular to the vector of the modulation field, and this minimizes modulation field distortion and coupling interferences with individual loops of the resonator. To further decrease these interferences each individual loop is connected to the balun through 1 pF capacitors (see Fig. 2). This arrangement serves as a high-pass filter and suppresses penetration of the field modulation frequency signal into the RF signal path.

In addition, by preventing the induction of eddy currents, the problems stemming from eddy current heating and vibrations caused by electro-mechanical coupling are largely suppressed.

This multi-loop coaxial cable resonator is conceptually analogous to multi-gap loop-gap resonator designs. Field homogeneity and EPR signal to noise ratio analysis has been analyzed by Pias-

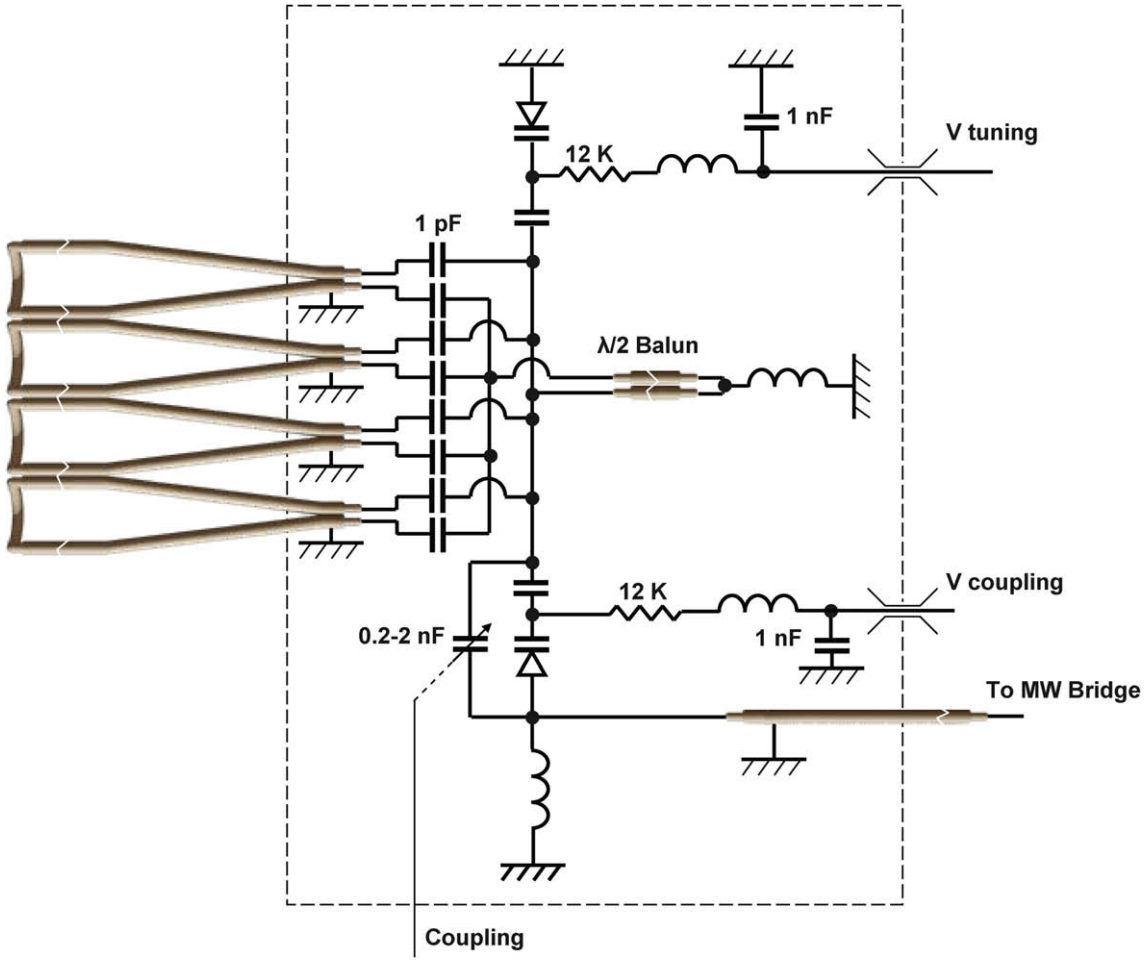

Fig. 2. Simplified equivalent diagram of matching circuit of the surface coil four-loop resonator. Changing of the capacitance of the variable capacitor allows initial matching of the input impedance to the characteristic impedance of the 50 Ω coaxial cable. Fine coupling and tuning is performed by changing capacitances of the corresponding varactor diodes.

ecki et al. for multi-gap loop-gap resonators [12]. It was shown that a proportional gain in signal intensity and homogeneity can be obtained as a function of number of gaps for lossy samples.

The coupling circuit used with this resonator uses electric coupling with varactor tuning and coupling provisions similar to the design reported by Hirata et al. [8,9]. Non-magnetic Silicon varactors (Infineon BB833) with 0.75–9.3 pF range of capacitance adjustment over 1–28 V control voltage range were employed. Parallel multi-feeder coupling allowed significant increase in loading capability necessary for achieving near-critical coupling to large lossy samples. In addition, the high symmetry of this coupling arrangement improves the homogeneity of the B_1 distribution of the resonator loaded with the lossy sample. In the present resonator, this design is modified to match four loops with the insertion of eight 1 pF capacitors as shown in Fig. 2.

3. Resonance frequency and dimensions

The equation for the resonator frequency is as follows:

$$\omega = 1/\sqrt{L_{sum}C_{sum}}$$

where

- $L_{\mathrm{sum}} = L * N$,
- L – inductance of the each loop (in general case with mutual inductance taken into account),
- $L = L_i + M$, L_i – Inductance of the individual loop,
- M – mutual inductance,
- C – capacitance of the individual gap,
- N – number of loops,
- $C_{sum} = C/N$.

This allows us to estimate the physical parameters of the resonator for a given frequency and number of loops.

The described segmented surface coil resonator design utilized four identical series connected segments. The capacitance of the individual gap is determined by the length of the shielded part of the coaxial cable. In our case, a 50 Ω cable has 1 pF capacitance per 10 mm length at 1.1 GHz frequency. So, to obtain 0.96 pF capacitance we took 9.6 mm length. This resulted in 0.48 pF capacitance for each gap as two cables connected in series. The addition of a coaxial cable feeding line equal to one half wavelength for phase inversion did not change the resonance frequency.

Equivalent inductance is determined by the geometry of the gap area, which was approximated as square consisting of four straight conductors 19 mm long and separated at the corners by 2.12 mm with $L = 0.174$ μH [16].

Final coaxial section lengths and capacitor values adjustments were performed to achieve the desired resonance frequency. We did not calculate the Q-factor since it may have a greater margin of error due to multiple factors not considered in the lumped circuit model such as radiation losses.

4. Testing and results

Sensitivity profile (B_1 field distribution) of surface resonators was considered in [9]. RF magnetic field magnitude decreases exponentially as function of the distance from the plane of resonator loop. In the 4.5 mm diameter single loop resonator described in [13], the practical limit for distance from the plane of resonator surface is reported to be about 3 mm.

We have measured the absolute intensity of the B_1 field distribution as a function of distance from the plane of the resonator surface utilizing a small (3.3 mm diameter) brass sphere using perturbing spheres method [17]. The measurement of B_1 field distribution was performed in the resonator loaded with 40 mm diameter cylinder filled with 0.5 mm glass spheres. Voids between glass spheres were filled with saline solution. This phantom simulates tissue load and allowed free positioning of the brass sphere. The brass sphere was cemented to a quartz rod and its position was controlled by a micro positioning device.

For sensitivity comparison purposes similar measurements were performed using an 8-mm commercial surface coil. Direct sensitivity comparison with the single loop resonator is not feasible on samples larger or deeper than the loop diameter because single loop resonator can not accommodate or fully cover these larger volumes. The 8 mm commercial surface coil resonator manufactured by Magnetech, GmbH is the closest coil for comparison available to us capable of coupling to the surface of a large lossy sample at this frequency. Frequency shift was monitored using an Agilent 8719ES vector network analyzer at 3.2 mW power.

The measurement results are shown in Fig. 3. Compared to the SSCR, the B_1 field distribution shows stronger B_1 field for the Magnetech resonator at distances smaller than 5 mm from the coil plane. However, at distances more than 5 mm, SSCR demonstrates stronger B_1 field and outperforms the single loop gap resonator. From Fig. 3, one can envision that the commercial resonator may have better sensitivity at distance less than 5 mm from the plane of the loop. However, at bigger distances the SSCR will outperform it. It should be noted that the magnitude of B_1 field at a point does not serve as an effective criteria of the overall resonator efficiency. Instead, we propose that a better criterion for comparing resonator efficiency of different design and size should include an integral of B_1 over the active volume of the resonator. Also, given sample properties will influence the individual sensitivity.

The microwave properties of the resonator were measured using Agilent 8719ES S Parameter Network Analyzer. The *Q*-factor of the empty critically coupled resonator was 300. The *Q*-factor of the resonator with an 18-mm diameter cylindrical bottle, 40 mm length, filled with water, inserted into the center of resonator dropped to 120. The same amount of Dulbecco's phosphate-buffered saline 50% solution sample or 100% normal Dulbecco's phosphate-buffered sample saline decreased the *Q* to 55 or 50, correspondingly. It is important that the resonator allowed critical coupling even with lossy samples of considerable volume.

In order to assess the applicability of the resonator for slice selective experiments and plane selectivity, a phantom assembly consisting of a 20-mm long cluster of 86 capillary glass tubes (cut out of 100 μL glass pipettes ID = 1.1 mm, OD = 1.7 mm) bound together into a octagonal shape was constructed. The tubes were filled with 1 mM solution of TEMPONE (2,2,6,6-tetramethyl-4-

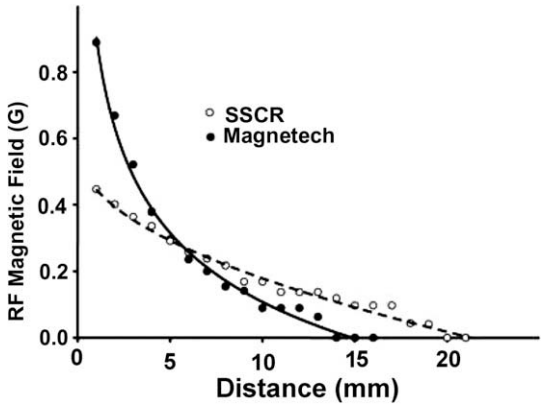

Fig. 3. Drop off of the B_1 field from the center of the SSCR versus distance from the resonator plane (open circles). Measurements were performed using a 3.3-mm diameter brass sphere. For comparison, similar measurements were performed for a conventional single loop surface-coil resonator, 8-mm Magnetech resonator (solid circles).

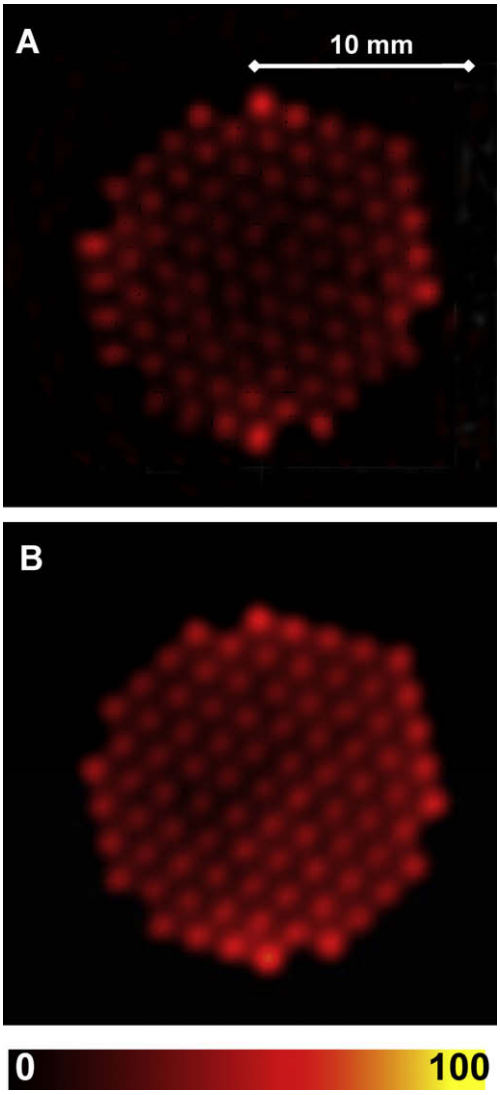

Fig. 4. (A) Middle slice of 3D EPR image of the phantom consisting of 86 capillary tubes of 1.1 mm inner/1.7 mm outer diameter filled with 1 mM TEMPONE used for RF field homogeneity assessment. The parameters used for the EPRI acquisition were as follows: frequency 1.1 GHz, microwave power ~200 mW, modulation amplitude 0.05 mT at 100 kHz, scan width 2.4 mT field gradient 0.1 T/m, scan time 9.1 s, 46×46 projections, field of view $24 \times 24 \times 24$ mm, reconstruction size $128 \times 128 \times 128$ voxels, slice thickness 0.19 mm. (B) 2D image of the same phantom. The parameters used for the EPRI acquisition were as follows: frequency 1.1 GHz, microwave power 200 mW, modulation amplitude 0.044 mT at 100 kHz, scan width 2.4 mT, field gradient 0.1 T/m, scan time 5.5 s, 512 projections, field of view 24×24 mm.

oxopiperidine-1-oxyl), spin probe commonly used for biological applications [2,18,19]. This phantom allowed testing the sensitivity and homogeneity of B_1 field distribution in the plane of the resonator coil with these small discrete sample tubes (Fig. 4).

The usable volume of the SSCR together with homogeneity of the EPR signal intensity over the surface of the four-loop SSCR that is critical for topical applications was evaluated with three-dimensional spatial imaging [15]. To assist evaluation, a special phantom was constructed. The phantom was a 40-mm outer diameter cylinder with flat 0.5 mm thick bottom end surface, providing a minimum 0.5 mm separation between phantom liquid and the resonator. This end surface thickness simulates the distance between resonator and subject tissue typically used in open chest heart measurements [20]. The cylinder was filled with 100 μM solution of TEMPONE (0.06 mT linewidth) in saline. The concentration was chosen in order demonstrate sensitivity in potential in vivo experiments. Image reconstruction was performed as previously described [21,22]. The size of the phantom exceeded the active volume of the resonator and, thus the obtained images represented the active volume of the resonator. Vertical and horizontal slices of a three-dimensional image of this quasi-infinite sample positioned on the surface of the resonator are shown in Fig. 5A. B_1 field profiles obtained from images confirm good signal distribution in the *XY* plane (Fig. 5A) as well as about 10 mm penetration along the *Z*-direction (Fig. 5B). Usable volume is defined as volume where signal was above noise threshold. Volume with lesser intensity was zeroed.

Comparison of signal distribution between Figs. 4 and 5 demonstrates quite different pattern. For the images shown in Fig. 4, the signal seems to increase with the position moving near the resonator loop. However, from the image shown in Fig. 5A, higher intensities are observed toward the center of the resonator loop. These variations are the result of the effect of the sample structure on the microwave field distribution. This effect is observed when the size of the sample is comparable with the microwave wavelength in the sample. Homogeneous load with high dielectric constant tends to "concentrate" the magnetic field resulting in higher concentrations observed around the center of the resonator loop. This effect is much less noticeable with the dispersed load of the discrete capillary tubes.

To evaluate the applicability of the resonator for in vivo applications, images of rats injected i.p. with a paramagnetic charcoal oximetry probe suspension were performed. Female rats of about 250 g weight were obtained from Charles River Laboratories (Wilmington, MA). All measurements were performed under ketamine/xylazine anesthesia (200 mg/kg and 4 mg/kg, respectively, i.p.). The anesthesia was maintained for a period of ~1 h – enough to acquire a series of EPRI and proton MRI images. The rats were prepared by injecting of 1.5 cc of suspension of the charcoal EPR probe (Activated Carbon, Darco® KB-B, −100) in 1:10 proportion by weight with aqueous solution of 5% glucose. Imaging was performed on the EPR/NMR co-imaging system with modified resonator setup [23]. The SSCR was positioned coaxially in the plane of the MRI coil to exclude the need for the moving stage previously required for

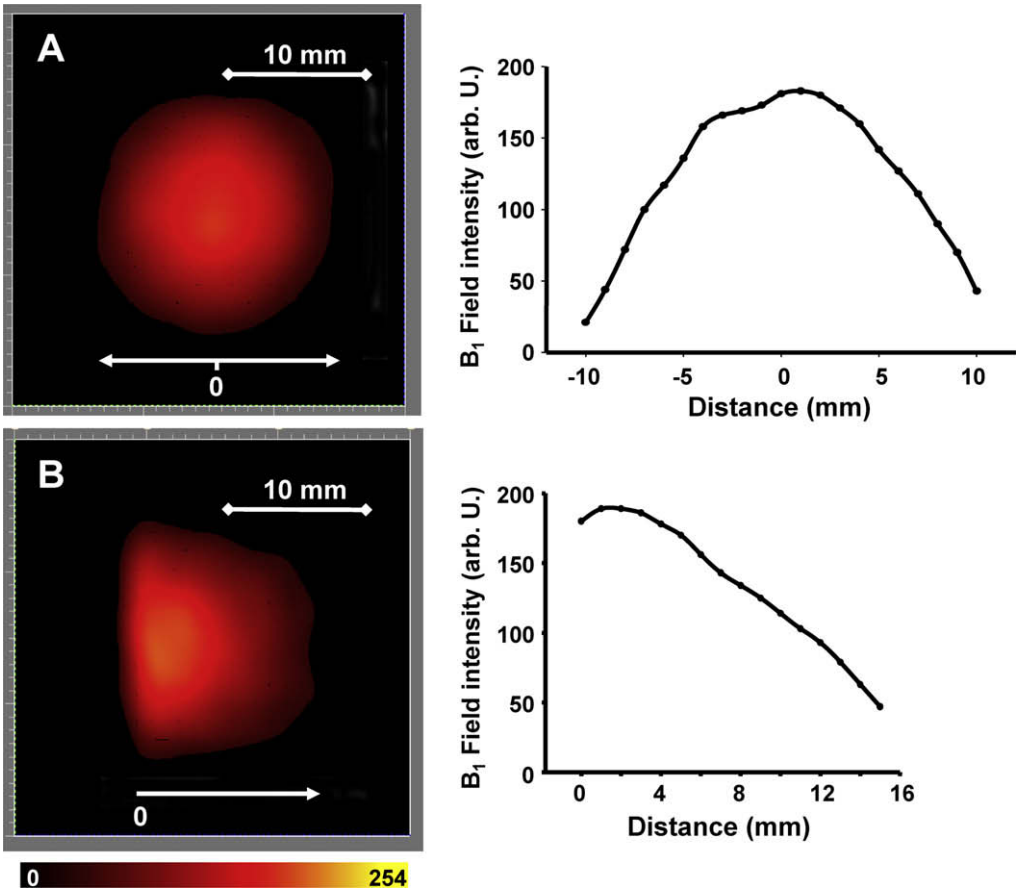

Fig. 5. Left: slices of 3D EPR image of the flat bottom tube filled with 100 μM TEMPONE solution (linewidth 0.06 mT) in normal saline. The 26 mm tube was filled to the height of 30 mm and its bottom was placed on the surface of the resonator. Right: profiles of B_1 field calculated from corresponding slice of the EPR image. (A) Central vertical slice of the image. (B) Horizontal slice 1 mm above the bottom of the tube. The parameters used for the EPRI acquisition were as follows: frequency 1.1 GHz, microwave power ~300 mW, modulation amplitude 0.05 mT at 100 kHz, field gradient 0.05 T/m, scan time 2.6 s, 32 × 32 projections, scan width 1.5 mT.

positioning separate EPRI/MRI resonators. The rat was placed on its side and the resonator was placed over the abdomen in the region of the injection. This arrangement allowed efficient coupling with both EPR and NMR resonators on the living rat. Resultant EPR/MRI images demonstrate that the SSCR allows mapping of paramagnetic density up to 20 mm in tissue depth (Fig. 6).

5. Summary and conclusions

A four-loop segmented surface coil resonator (SSCR) design with loop diameter of 20 mm and increased aperture, for EPR spectroscopy and imaging of biological samples at 1.1 GHz was designed and constructed. This resonator has greater depth of penetration than conventional single loop resonators, for this frequency and it allows detection from deeper layers up to 20 mm in tissue depth. The resonator has good RF magnetic field homogeneity that was achieved by symmetrical multi-loop geometry. Both mechanical and electrical designs of the resonator provide high transparency and uniformity for magnetic modulation field, as well as mechanical rigidity. The design provides high sensitivity, ease of sample access, excellent electrical stability, and good B_1 field homogeneity suitable for in vivo EPR spectroscopy and imaging. Effective separation of the electric component of the microwave field from the active volume decreases Q-factor degradation in the presence of a lossy biological sample, hence, contributing to better sensitivity and coupling capability. Resonator ATC and ACC circuitry containing varactor diodes provided electronic coupling and tuning over a wide range of sample loading conditions. The SSCR design can be used for surface applications or as a slice selective volume resonator and enables larger objects to be studied than possible with conventional SCRs. The open structure and enhanced distribution of RF field homogeneity of the SSCR over a surface or slice volume makes it suitable for EPR spectroscopy and imaging of in vivo animals and isolated organs at higher microwave frequencies.

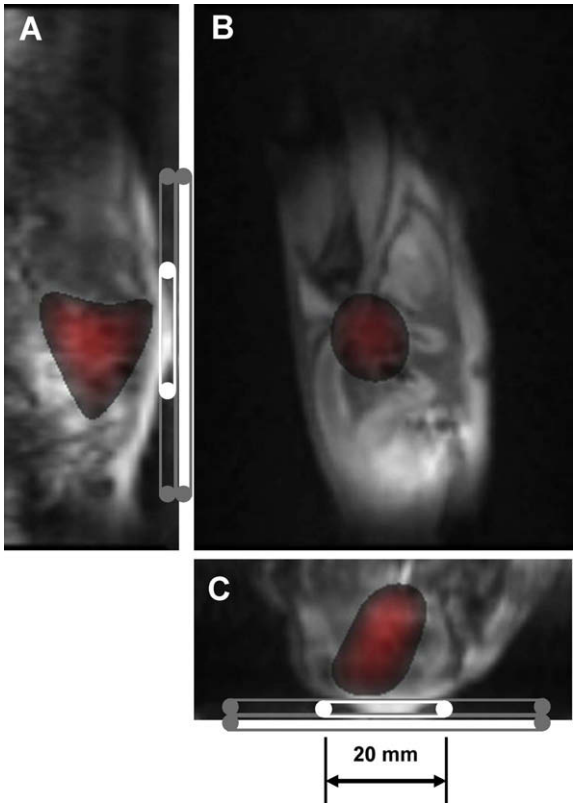

Fig. 6. Slices of 3D EPR images from a live rat injected i.p. with paramagnetic charcoal suspension (rendered in hot metal color scale) shown fused with proton MRI (rendered in gray scale). The images show the rat positioned with head at bottom. (A) Sagital slice, (B) coronal slice and (C). White outline shows approximate position of the SSCR on the surface of the rat, gray outline shows NMR coil (see A and C). The MRI data was acquired, using gradient echo pulse sequence with the following parameters: 12.5 kHz bandwidth, matrix $128 \times 128 \times 128$, repetition time T_R = 230 ms, echo delay time T_E = 13 ms, number of excitations (NEX) = 1, field of view (FOV) in plane 80×80 mm, FOV in slice direction 80 mm (transverse slice thickness of 0.625 mm), flip angle 90 degrees. Total acquisition time was 32 min. The parameters used for the EPRI acquisition were as follows: frequency 1.075 GHz, microwave power 300 mW, modulation amplitude 0.16 mT, scan width 8 mT, field gradient 0.1 T/m along all directions, projection number 24×24, scan time 1.3 s, total acquisition time 14 min. Images shown are cropped from the full $80 \times 80 \times 80$ mm FOV.

Acknowledgments

This work was supported by NIH Research Grants EB0890 and EB4900.

References

[1] J.L. Berliner, H. Fujii, Magnetic resonance imaging of biological specimens by electron paramagnetic resonance of nitroxide spin labels, Science 227 (1985) 517–519.
[2] J.L. Zweier, P. Kuppusamy, Electron paramagnetic resonance measurements of free radicals in the intact beating heart: a technique for detection and characterization of free radicals in whole biological tissues, Proc. Natl. Acad. Sci. USA 85 (1988) 5703–5707.
[3] T. Yoshimura, H. Yokoyama, S. Fujii, F. Takayama, K. Oikawa, H. Kamada, In vivo EPR detection and imaging of endogenous nitric oxide in lipopolysaccharide-treated mice, Nat. Biotechnol. 14 (1996) 992–994.
[4] H.M. Swartz, H.J. Halpern, EPR studies of living animal and related model systems (in vivo EPR), in: L.J. Berliner (Ed.), Spin Labeling: The Next Millennium, Plenum Press, New York, 1998, pp. 367–397.
[5] G. He, R.A. Shankar, M. Chzhan, A. Samouilov, P. Kuppusamy, J.L. Zweier, Noninvasive measurement of anatomic structure and intraluminal oxygenation in the gastrointestinal tract of living mice with spatial and spectral EPR imaging, Proc. Natl. Acad. Sci. USA 96 (1999) 4586–4591.
[6] V.V. Khramtsov, I.A. Grigor'ev, M.A. Foster, D.J. Lurie, In vitro and in vivo measurement of pH and thiols by EPR-based techniques, Antioxid. Redox Signaling 6 (2004) 667–676.
[7] S. Petryakov, A. Samouilov, E. Kesselring, T. Wasowicz, G. Caia, J.L. Zweier, Single loop – multi gap resonator for whole body EPR imaging of mice at 1.2 GHz, J. Magn. Reson. 188 (2007) 68–73.
[8] H. Hirata, G. He, Y. Deng, I. Salikhov, S. Petryakov, J.L. Zweier, A loop resonator for slice-selective in vivo EPR imaging in rats, J. Magn. Reson. 190 (2008) 124–134.
[9] H. Hirata, T. Walczak, H.M. Swartz, Characteristics of an electronically tunable surface-coil-type resonator for L-band electron paramagnetic resonance spectroscopy, Rev. Sci. Instrum. 72 (2001) 2839–2841.
[10] H. Hirata, T. Walczak, H.M. Swartz, Electronically tunable surface-coil-type resonator for L-band EPR spectroscopy, J. Magn. Reson. 142 (2000) 159–167.
[11] I. Salikhov, H. Hirata, T. Walczak, H.M. Swartz, An improved external loop resonator for in vivo L-band EPR spectroscopy, J. Magn. Reson. 164 (2003) 54–59.
[12] W. Piasecki, W. Froncisz, Field distributions in loop-gap resonators, Meas. Sci. Technol. 4 (1993) 1363–1369.
[13] K. Takeshita, T. Takajo, H. Hirata, M. Ono, H. Utsumi, In vivo oxygen radical generation in the skin of the protoporphyria model mouse with visible light exposure: an L-band ESR study, J. Invest. Dermatol. 122 (2004) 1463–1470.
[14] P. Kuppusamy, M. Chzhan, K. Vij, M. Shteynbuk, D.J. Lefer, E. Giannella, J.L. Zweier, Three-dimensional spectral-spatial EPR imaging of free radicals in the heart: a technique for imaging tissue metabolism and oxygenation, Proc. Natl. Acad. Sci. USA 91 (1994) 3388–3392.
[15] G. He, S.P. Evalappan, H. Hirata, Y. Deng, S. Petryakov, P. Kuppusamy, J.L. Zweier, Mapping of the B1 field distribution of a surface coil resonator using EPR imaging, Magn. Reson. Med. 48 (2002) 1057–1062.
[16] M.D.A. Bueno, A.K.T. Assis, Inductance and force calculations in electrical circuits, Nova Science Publishers, Inc., 2001.
[17] J.H. Freed, D.S. Leniart, J.S. Hyde, Theory of saturation and double resonance effects in ESP spectra. RF coherence and line shapes, J. Chem. Phys. 47 (1967) 2762–2773.
[18] P. Kuppusamy, P. Wang, J.L. Zweier, Evaluation of nitroxides for the study of myocardial metabolism and oxygenation, Magn. Reson. Chem. 33 (1995) 123–128.
[19] G. He, A. Samouilov, P. Kuppusamy, J.L. Zweier, In vivo EPR imaging of the distribution and metabolism of nitroxide radicals in human skin, J. Magn. Reson. 148 (2001) 155–164.

[20] X. Zhao, G. He, Y.R. Chen, R.P. Pandian, P. Kuppusamy, J.L. Zweier, Endothelium-derived nitric oxide regulates postischemic myocardial oxygenation and oxygen consumption by modulation of mitochondrial electron transport, Circulation 111 (2005) 2966–2972.
[21] Y. Deng, G. He, P. Kuppusamy, J.L. Zweier, Deconvolution algorithm based on automatic cutoff frequency selection for EPR imaging, Magn. Reson. Med. 50 (2003) 444–448.
[22] P. Kuppusamy, J.L. Zweier, A forward-subtraction procedure for removing hyperfine artifacts in electron paramagnetic resonance imaging, Magn. Reson. Med. 35 (1996) 316–322.
[23] A. Samouilov, G.L. Caia, E. Kesselring, S. Petryakov, T. Wasowicz, J.L. Zweier, Development of a hybrid EPR/NMR co-imaging system, Magn. Reson. Med. 58 (2007) 156–166.